High sampling-rate measurement of turbulence velocity fluctuations in Mach 1.8 Laval jet using interferometric Rayleigh scattering*

Li Chen(陈力)†, Fu-Rong Yang(杨富荣), Tie Su(苏铁), Wei-Yi Bao(鲍伟义), Bo Yan(闫博), Shuang Chen(陈爽), and Ren-Bing Li(李仁兵)

China Aerodynamics Research and Development Center, Mianyang 621000, *China*

(Received 4 October 2016; revised manuscript received 8 November 2016; published online 10 January 2017)

Interferometric Rayleigh scattering diagnostic technique for the time-resolved measurement of flow velocity is studied. Theoretically, this systematic velocity-measured accuracy can reach up to 1.23 m/s. Measurement accuracy is then evaluated by comparing with hot wire anemometry results. Moreover, the distributions of velocity and turbulence intensity in a supersonic free jet from a Laval nozzle with a Mach number of 1.8 are also obtained quantitatively. The sampling rate in this measurement is determined to be approximately 10 kHz.

Keywords: Fabry–Pérot interferometer, Rayleigh scattering, time-resolved velocity measurement, turbulence

PACS: 52.38.Bv, 42.65.Es, 47.60.Kz, 47.85.Gj **DOI:** 10.1088/1674-1056/26/2/025205

1. Introduction

Velocity measurements in a flow field have attracted significant attention in the development of aerospace technology and aerodynamics.[1,2] Previous measurement systems have tended toward hot wire/ hot film anemometry,[3] time-resolved particle image velocimetry (TR-PIV),[4] and laser Doppler velocimetry (LDV).[5,6] Hot wire/hot film anemometry, along with contact gauges, has always been used in subsonic and transonic speed fluidic velocity measurements. The TR-PIV and LDV, which are based on tracer particles, have been developed for steady flow velocity measurement. However, their precision is affected by particle-adding technology and trace particle-following features, which restricts their development and application in unsteady flow velocity measurements.

Knowledge of interferometric Rayleigh scattering (IRS) dates back to the 20th century. It is mainly based on a Fairy–Pérot (F-P) interferometer, which is used to discriminate the Rayleigh scattering (RS) spectrum accurately.[7–10] Then, IRS can be used for the non-contact measurement of flow velocity, flow temperature, and gas density.[11–14] Recently, many institutes have successfully used photomultiplier detectors to achieve RS signals. The Glenn Research Center of NASA reported that interferometric rings that corresponded to RS were imaged by using different photomultipliers, and the spectral profile and flow velocity were then acquired via complicated picture-processing arithmetic.[15–20] Although the amplification factor of a photomultiplier was large, spectral rings were obtained by using only a few photomultipliers, thereby reducing the spatial sampling rate of the IRS apparatus. To improve the spatial sampling rate, an intensified charge-coupled device (ICCD) was used to image interferometric rings for measuring the instantaneous velocity of flow.[21,22] However, the systematic temporal sampling frequency was only 10 Hz.

In this study, we demonstrate a measurement system with a high temporal and spatial sampling rate. This system is mainly fabricated based on an F-P interferometer and an electron-multiplying charge-coupled device (EMCCD). Temporal sampling frequency can increase up to 10 kHz, ensuring high spatial sampling frequency. The spectral results suggest that this system can be generalized to the measurement of high-precision velocity and turbulence intensity in supersonic flow.

2. Theory

An incident light interacts with an atom or a molecule, thereby inducing a dipole moment that oscillates and radiates at the frequency of the incident field. This phenomenon is considered as an elastic scattering process because the internal energy of molecules remains unchanged, whereas the frequency of light is changed only via the Doppler effect given bulk motion of molecules. Doppler shift $\Delta\nu_{\mathrm{D}}$ can be given by[21]

$$\Delta\nu_{\mathrm{D}} = \frac{1}{\lambda}(\boldsymbol{S}-\boldsymbol{L})\cdot\boldsymbol{V} = \frac{2\sin(\theta/2)}{\lambda}V_k, \tag{1}$$

where λ is the wavelength of the incident light; $\boldsymbol{V}$ is the velocity of gas motion; θ represents the angle between the direction of the incident light and that of the scattered light; $\boldsymbol{L}$ and $\boldsymbol{S}$ are the wave vectors of the incident light and the scattered light, respectively. The measured velocity component, V_k is in the same direction as $\boldsymbol{S}-\boldsymbol{L}$ (Fig. 1).

The minimal variation between the wavelengths of the incident light and the scattered light is attributed to Doppler

*Project supported by the National Natural Science Foundation of China (Grant No. 11272337).

†Corresponding author. E-mail: chenli_03@163.com

© 2017 Chinese Physical Society and IOP Publishing Ltd

shift. Taking gas velocity $V_k = 100$ m/s for example, when the incident light wavelength $\lambda = 532$ nm and the angle $\theta = 90°$, the wavelength shift from the incident light is only 2.5×10^{-5} nm according to Eq. (1). An F-P interferometer was recently used to resolve the RS spectrum.[23–26] When a parallel beam irradiates the F-P interferometer, sharp interferometric rings can be imaged once the condition is fulfilled, i.e.,[21]

$$\delta = \frac{4\pi}{\lambda} nh\cos i = 2k\pi, \tag{2}$$

where δ is the phase difference between two transmitted light beams; i is the angle between the light beam and the optical axis; n and h are the refractive index and F-P mirror spacing, respectively; k represents the order of the interferometric rings. When the wavelength λ and the focal distance of the lens f are considered, the radius of the interferometric ring r_k is related to the interferometric ring order k according to[21]

$$r_k \approx \sqrt{2 - \frac{k\lambda}{nd}} f. \tag{3}$$

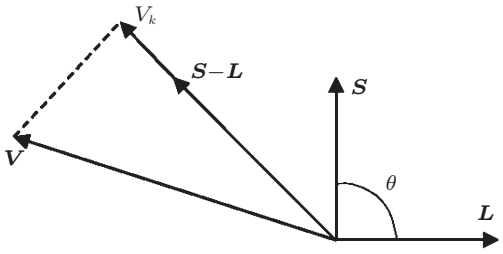


Fig. 1. Geometric sketch of Doppler frequency-shift.[20]

The radius of the ring of the scattered light can be inferred using Eq. (3) as follows:

$$r'_k \approx \sqrt{2 - \frac{k(\lambda + \Delta\lambda)}{nd}} f. \tag{4}$$

Flow velocity turbulence intensity I is then given by[16]

$$I = \frac{1}{\bar{V}} \sqrt{\frac{1}{N} \sum_{i=1}^{N} (V_i - \bar{V})^2}. \tag{5}$$

3. Experimental setup

The optical arrangement of the time-resolved IRS (TIRS) system is shown in Fig. 2. A coherent 10-W continuous-wave (CW) 532-nm laser with a 2-mm-diameter and 5-MHz linewidth output beam provides the incident light for the system. A small portion of laser energy is extracted by using a beam splitter, to serve as the reference light during measurements. Most of the laser beam is focused by using a 1000-mm focal length lens (L1) into a spot with a diameter of 100 μm at the probe volume. The beam is oriented at an angle of 45° with respect to the primary flow direction, whereas the scattered light is collected at an angle of 90° relative to the incident laser beam. A finite length of the scattered light is imaged by using a pair of lenses (L2 and L3) onto the face of a multimode optical fiber with a diameter of 1 mm. The scattered light and the reference light are then combined via the Y fiber and irradiated parallel to the F-P interferometer. Subsequently, interferometer rings are focused and imaged on EMCCD as shown in Fig. 3(a). The radius of the ring clearly varies between the scattered light and the reference light because of Doppler shift. The corresponding flow velocity V_k can be finally obtained according to Eqs. (1), (3), and (4).

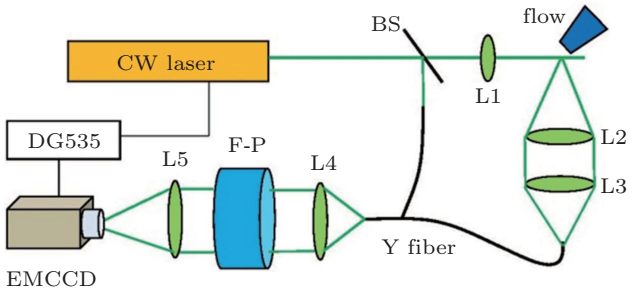


Fig. 2. (color online) Sketch of the TIRS system.

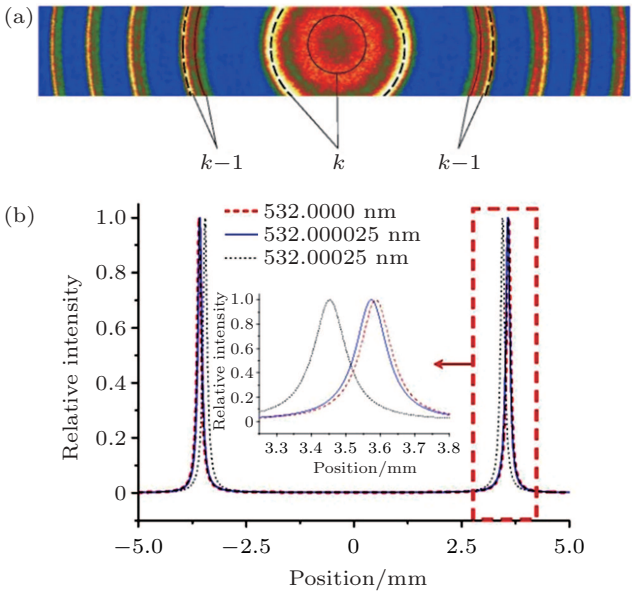


Fig. 3. (color online) (a) Interference rings consist of the reference laser (black dotted lines) and the Rayleigh light (black solid lines) scattered simultaneously at different levels (k, $k-1$). (b) Computational one-dimensional (1D) intensity distributions of F-P interference rings at different laser wavelengths. The inset shows a partially enlarged view.

4. Results and discussion

To characterize the interferometric information according to different wavelengths, 1D distributions of interferometric rings at different wavelengths (532.0000, 532.000025, and 532.00025 nm) are simulated as shown in Fig. 3(b). The aperture and surface reflectivity of the F-P interferometer are set to be 50 mm and 90%, respectively. The focal length of the L5 lens is 1000 mm. The laser linewidth and the angle θ are determined to be 5 MHz and 90°, respectively. The ring radius

decreases with the increase of wavelength. Taking the wavelengths 532 nm and 532.000025 nm for example, the peak separation between the two spectra is approximately 13 μm as shown in the inset of Fig. 3(b), whereas the optimized pixel size is approximately 1.6 μm in the EMCCD image. Hence, velocity resolution in the designed TIRS system can theoretically reach up to 1.23 m/s.

Then, the property of the designed velocity and turbulence intensity measurement system (as shown in Fig. 2) is experimentally realized. Hot wire anemometry is performed and the results are compared with those of the designed system by measuring velocity and turbulence intensity in the same Laval nozzle (Mach number: 1.8). In the measurements, the two apparatuses are independently operated at the same position, that is, 80 mm away from the entrance of the nozzle and 1.5 mm away from the axis of flow. Then, the sampling rate and the sampling time are set to be 5 kHz and 3 s, respectively. Furthermore, inlet pressure is approximately 0.7 MPa. The difference in measured velocity between the hot wire system and the designed system, and the corresponding power results are clearly seen in Figs. 4 and 5, respectively. The distinction between the two apparatuses is small, that is, the velocity and turbulivity results are (280 m/s, 7.08%) and (291 m/s, 6.9%), respectively (as listed in Table 1). Therefore, the designed TIRS system can be used further to measure the flow velocity and turbulence.

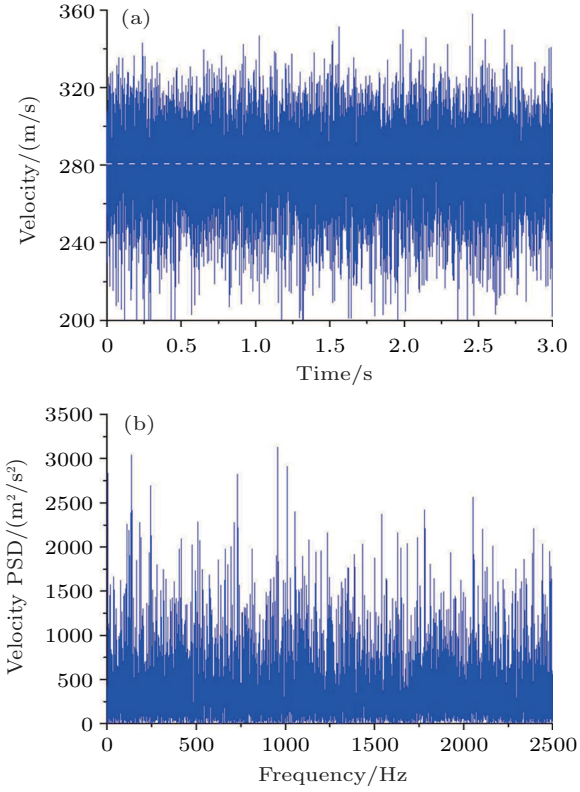


Fig. 4. (color online) (a) Velocity pulsation and (b) power spectrum density (PSD) measured via hot wire anemometry.

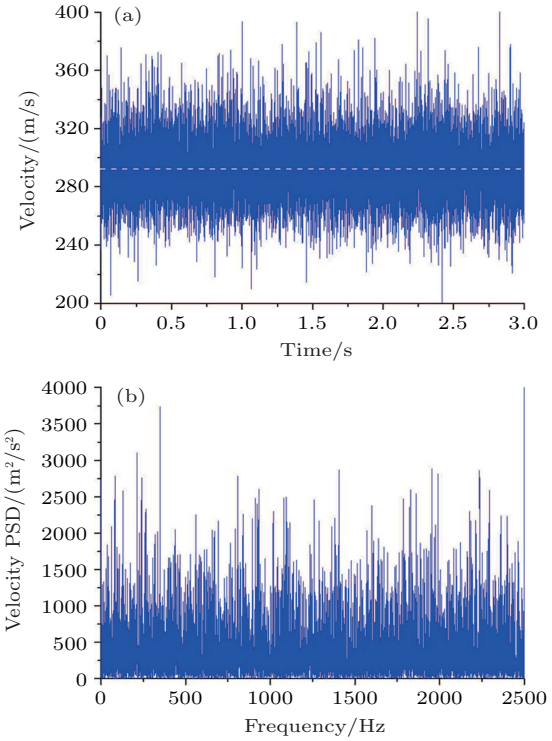


Fig. 5. (color online) (a) Velocity pulsation and (b) PSD measured by using the TIRS system.

Table 1. Measured velocity and turbulence relating to Figs. 4 and 5.

	Hot wire	Designed apparatus
Average velocity/(m/s)	280	291
Turbulence	7.08%	6.98%

Subsequently, TIRS measurement is performed during the testing of a supersonic free jet produced by a Laval nozzle with a Mach number of 1.8. The sampling rate is set to be 10 kHz, and the other evaluation parameters are the same as those mentioned earlier. Prior to the measurement, the schisophone result of the nozzle is obtained to display its flow structure (Fig. 6). A stable flow can be achieved by reducing the distance to the entrance of the nozzle d_1. Then, the TIRS apparatus is used to measure the velocity and turbulence intensity distribution of the nozzle (Table 2). The detecting position is on the axis of flow. First, the change in flow velocity is slow at d_1 smaller than 30 mm, and turbulence intensity is relatively stable ($< 1.5\%$). Second, flow velocity clearly decreases with the increase of distance d_1. Third, turbulence intensity is well consistent with the increasing rule. That is, turbulence intensities are at 2.33%, 2.63%, and 4.98% for distance d_1 values of 40, 50, and 60 mm, respectively.

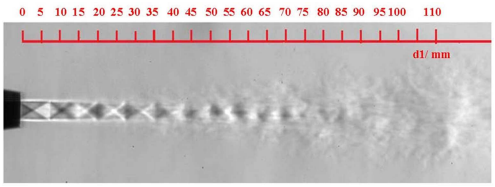


Fig. 6. (color online) Shadow graph of the free jet.

Table 2. Measured velocity and turbulence intensity results relating to distance d_1.

d_1/mm	10	15	20	30	40	50	60	70	80	90	100	110
Velocity/(m/s)	518	546	509	518	471	422	402	386	336	318	295	279
Turbulence/%	1.25	1.4	1.2	1.25	2.33	2.63	4.98	5.39	6.98	8.98	9.0	10.27

5. Conclusions and perspective

A TIRS apparatus for measuring flow velocity and turbulence intensity is designed in this study. The systematic sampling rate can increase to 10 kHz because of EMCCD. The theoretical results show that the velocity resolution of TIRS can reach 1.23 m/s. Further experiments verify that this test system can be used to measure flow velocity and turbulence. Moreover, this apparatus is used to quantitatively measure the velocity and the turbulence distribution of the Laval nozzle. The result is similar to that of a schisophone. By further studing the change in Rayleigh-scattered signals influenced by flow temperature and gas density, the multifunctional apparatus will be used to measure various flow parameters, such as temperature and gas density.

References

[1] He L, Yi S H, Tian L F, Chen Z and Zhu Y Z 2013 *Chin. Phys. B* **22** 024704

[2] Amy F, Mielke R G, Seasholtz K A and Elam J P 2005 *Exp. Fluids* **39** 441

[3] Ardekani M A and Motlagh M M 2010 *Measurement* **43** 31

[4] Kaffelabc A, Moureha J, Harionbc J L and Russeilbc S 2016 *Exp. Therm. Fluid Sci.* **77** 71

[5] Dorothea I, Hollnagel M, Paul E, Summers P, Spyros S, Kollias M and Dimos P P 2007 *J. Magn. Reson. Imaging* **26** 1493

[6] Yeh Y and Cummins H Z 1964 *Appl. Phys. Lett.* **4** 173

[7] Lock J A, Seasholtz R G and John W T 1992 *Appl. Opt.* **31** 2839

[8] Seasholtz R G, Zupanc F J and Schneider S J 1992 *J. Propulsion and Power* **8** 935

[9] Andres N, Arroyo P and Quintanilla M 1997 *Appl. Opt.* **36** 6997

[10] Seasholtz R G and Greer L C 1998 "Rayleigh scattering diagnostic for measurement of temperature and velocity in harsh environments", *AIAA* 36*th Aerospace Sciences Meeting and Exhibition*, January 12–15, 1998, Reno, NV, p. 0206

[11] Bivolaru D, Danehy P M, Gaffney R L Jr and Cutler A D 2008 "Direct-view multi-point two-component interferometric Rayleigh scattering velocimeter", *AIAA* 46*th Aerospace Sciences Meeting and Exhibition*, January 9–12, 2008, Reno, NV, p. 0236

[12] Bivolaru D, Danehy P M and Lee J W 2006 *Opt. Lett.* **31** 1645

[13] Bivolaru D, Danehy P M, Lee J W, Gaffney R L Jr and Cutler A D 2006 "Single-pulse Multi-point Multi-component Interferometric Rayleigh Scattering Velocimeter", *AIAA* 44*th Aerospace Sciences Meeting and Exhibition*, January 9–12, 2006, Reno, NV, p. 0836

[14] Mielke A F, Clem M M and Elam K A 2010 "Rayleigh scattering measurements using a tunable liquid crystal Fabry-Perot interferometer", *AIAA* 27*th Aerodynamic Measurement Technology and Ground Testing Conference*, June 28–July 1, 2010, Chicago, Illinois, USA, p. 4350

[15] Mielke A F and Elam K A 2009 *Exp. Fluids* **47** 673

[16] Seasholtz R G, Panda J and Elam K A 2001 "Rayleigh scattering diagnostic for dynamic measurement of velocity fluctuations in high speed jets", *AIAA* 39*th Aerospace Sciences Meeting & Exhibition*, January 8–11, 2001, Reno, NV, p. 0847

[17] Seasholtz R G, Panda J and Elam K A 2002 *AIAA* 40*th Aerospace Sciences Meeting & Exhibition*, January 14–17, 2002, Reno, NV, p. 0827

[18] Mielke A F, Seasholtz R G, Elam K A and Panda J 2005 *Exp. Fluids* **39** 441

[19] Mielke A F and Elam K A 2006 "Rayleigh Scattering Diagnostic for Measurement of Temperature, Velocity, and Density Fluctuation Spectra", *AIAA* 44*th Aerospace Sciences Meeting & Exhibition*, January 9–12, 2006, Reno, NV, p. 0837

[20] Mielke A F and Elam K A 2009 *AIAA journal* **47** 850

[21] Chen L, Yang F R, Su T, Bao W Y, Qi X H and Chen S 2015 *Acta Photon. Sin.* **44** 0112004

[22] Amy F F, Michelle M C and Kristie A E 2012 "Improvement in Rayleigh Scattering Measurement Accuracy", *AIAA* 50*th Aerospace Sciences Meeting Including the New Horizons Forum and Aerospace Exposition*, January 9–12, 2012, Nashville, Tennessee, p. 1060

[23] Seasholtz R G and Panda J 2000 "Rayleigh Scattering Diagnostic for Simultaneous Measurements of Dynamic Density and Velocity", *AIAA* 38*th Aerospace Sciences Meeting & Exhibition*, January 10–13, 2000, Reno, NV, p. 0642

[24] Xia H Y, Dou X K, Sun D S, Shu Z F, Xue X H, Han Y, Hu D D, Han Y L and Cheng T D 2012 *Opt. Express* **20** 15286

[25] Xia H Y, Dou X K, Shangguan M J, Zhao R C, Han Y L, Shu Z F, Xue X H, Han Y, Wang C and Qiu J W 2014 *Opt. Express* **22** 21775

[26] Xia H Y, Shangguan M J, Wang C, Shentu G L, Qiu J W, Zhang Q, Dou X K and Pan J W 2016 *Opt. Lett.* **41** 5218